Superconducting pairing symmetry and spin-orbit coupling in proximitized graphene

Abdulrhman M. Alsharari[1,*] and Sergio E. Ulloa[2]
[1]*Department of Physics, University of Tabuk, Tabuk, 71491, Saudi Arabia*
[2]*Department of Physics and Astronomy, and Nanoscale and Quantum Phenomena Institute, Ohio University, Athens, Ohio 45701, USA*

(Received 26 May 2020; revised 30 July 2020; accepted 3 September 2020; published 21 September 2020)

Graphene may exhibit different topological phases as a result of proximity to different substrates. We study the effect of superconductivity in such systems using the effective Bogolyubov-de Gennes Hamiltonian with different superconducting pairing order parameters. We analyze the topological phase transition and symmetry class of the system in different parameter regimes. A particularly interesting situation occurs when nearest-neighbor spin-singlet superconducting pairing is present in phases of proximitized graphene that exhibit either inverted band or quantum spin Hall behavior. Both superconducting phases show similar characteristics in the low-energy range, including the appearance of robust edge states, and are neighboring phases across a transition that closes the quasiparticle gap as the chemical potential changes. Detailed construction and analysis of the existence and nature of edge states are presented in different system regimes.

DOI: 10.1103/PhysRevB.102.104509

I. INTRODUCTION

Graphene is distinguished by the existence of charge neutrality points where the density of states vanishes [1]. However, the Fermi level can be moved away from these Dirac points by doping or electrical gating, allowing for various possible behaviors to emerge, including different superconducting phases [2–5]. Possible pairing symmetries and order parameters have been investigated theoretically, based on different Hubbard models and approaches [3,6,7], resulting in a host of interesting phases.

Similarly, lattice inversion asymmetries introduced by applied fields [1] or proximity to nearly commensurate substrates may open gaps at the Dirac points [8]. As such, it is expected that proximity of graphene to a host of other monolayers or substrates would result in a rich spectrum with strong spin-orbit effects competing with the Dirac physics [9–12]. These proximitized properties would in turn affect and may even enhance the different superconducting phases in the hybrid graphene-multilayer system.

Significant interest is focused on topological superconductors, due to the intriguing properties of such systems [13–15]. Much progress also relies on the proximity effect, with different ways proposed to induce correlations in time-reversal invariant systems. One of these approaches places a nodeless *s*-wave superconductor in proximity to a semiconductor with strong spin-orbit coupling (SOC) to produce Majorana edge bound states [16]. Similarly, inducing superconductivity by proximity in silicene promises interesting properties [17]. Most important is the recent growing interest both experimentally and theoretically in studying bilayer graphene systems at low twisted angles, resulting in the appearance of superconducting and other interesting phases [12,18–20].

Prominent examples of materials to be used as substrate for graphene are transition-metal dichalcogenide (TMD) monolayers [9], as they are structurally and chemically the most stable as free monolayers, and the technology to create such hybrid structures is extremely well developed [21–23]. The quantum confinement in TMD monolayers yields a direct band gap at the corner points of their hexagonal Brillouin zone, while the heavy metal atoms generate an Ising-type SOC that preserves the S_z component [24]. The effect of SOC is observed on time-reversed spin-valley locking (K and K'), which can be seen as a pseudo-Zeeman field with opposite signs on each valley [25]. A similar pseudo-Zeeman field is transferred onto graphene via proximity to semiconducting TMDs [26–29], producing several additional terms in the low-energy Hamiltonian of the system. These terms strongly affect the dynamics, spin structure of the eigenstates, and even the topological character of the system [29,30]. Superconducting correlations in such interesting single-particle spectra have not been studied, especially as the role of pseudo-Zeeman effect and other competing interactions may have interesting consequences on the resulting superconductor.

Our work here focuses on the dynamical effects of considering various pairing symmetries or channels on the proximitized graphene's honeycomb structure over a range of chemical doping and pairing strengths. To achieve this, we write a proximitized graphene effective Hamiltonian to properly describe the SOC and staggered potential effects induced by its proximity to TMDs, and consider different superconducting pairings. We focus here on *s*-wave singlet and *f*-wave triplet pairing between nearest-neighbor sites (NN, atoms A and B in the unit cell), and between next-nearest neighbors (NNNs, sites A and A (or B and B) in neighboring cells), as examples of the simplest symmetries.

The competition of different materials or experimental conditions in the TMD-graphene hybrid results in single-particle states with different Berry curvatures and associated characteristics transferred onto graphene. The perturbations include

*aalsharari@ut.edu.sa

a staggered potential that breaks sublattice symmetry, as well as enhanced intrinsic and Rashba SOC that provide interesting spin texture to the eigenstates. It is the competition between these different interactions that results in a rich phase diagram for the hybrid multilayer, with three different regimes: *direct* band gap, *inverted mass,* and a topological insulator quantum spin Hall (QSH) phase [28,30,31]. (Note that the *inverted mass* regime is also referred to at times as *inverted bands* or *Mexican-hat bands* [10,28,29]; we use these terms interchangeably.) As we will show, the interplay of different band structure and superconducting pairing symmetries result in interesting ground states, which can be achieved by varying applied gate fields or chemical doping. We find that including NN s-wave correlations results in the system exhibiting a phase transition between distinct phases, separated by gap-closing conditions. The edge-state characterization of these two phases is correspondingly different, as one exhibits gapless edge states while the edges of the other are fully gapped. We are also able to calculate the Z_2 invariant of the different phases, using the classification for systems that preserve both time-reversal and charge conjugation, and find them to be in the same trivial category. The edge states are protected by the honeycomb lattice structure, but do not impart the system with topological protection in the superconducting regime. The interplay between different interactions in this structure leads to complicated correlated electron-hole dynamics, depending on the system features and conditions. For example, the QSH superconducting regime exhibits different spin-resolved quasiparticle (QP) states from those in the inverted band case. Also, states resulting from different superconducting order parameters (i.e., singlet or triplet pairings) show distinctive particle-hole admixtures, as will be shown in Figs. 3-5 (see Sec. III A).

We also see that shifts in the chemical potential create interesting modifications of these mixtures, as the modified correlations explore and exploit the different spin textures of the single-particle spectra. The resulting QPs in turn change the behavior of this hybrid system.

The paper is organized as follows. In Sec. II, we introduce the effective single-particle Hamiltonian for proximitized graphene and the different superconducting pairing symmetries we want to study via a Bogoliubov-de Gennes approach. In Sec. III A, we study the different QP spectra and characteristics under various superconducting pairing symmetries. Section III B reports on the topological structure of the spectra, and the associated edge states and zero-energy modes in finite-width ribbons of the material phase. Section III C discusses relevant experimental systems where superconductivity is realized. Finally, Sec. IV is devoted to conclusions and outlook.

II. MICROSCOPIC MODEL

The Bogoliubov-de Gennes Hamiltonian (BdG) [13,32] to describe superconducting pairing on the proximitized graphene system is given by

$$\mathcal{H}_{\rm BdG}(k) = \begin{pmatrix} \mathcal{H}_e(k) - \eta & \hat{\Gamma}(k) \\ \hat{\Gamma}^\dagger(k) & \mathcal{H}_h(k) + \eta \end{pmatrix}, \tag{1}$$

where $\mathcal{H}_e$ is the effective graphene tight-binding Hamiltonian that incorporates the effects of being in proximity of (deposited on) a TMD substrate and η is the chemical potential of the system. The $\hat{\Gamma}(k)$ matrix represents the pairing correlations in the system and will be described in Sec. II B below. The hole component is obtained from the electronic component as

$$\mathcal{H}_h(k) = -\mathcal{T}\mathcal{H}_e(k)\mathcal{T}^{-1}, \tag{2}$$

where $\mathcal{T}$ is the antiunitary time-reversal operator [13,32]. The BdG spinors are written in the A and B sublattice and spin basis

$$\Psi_k^\dagger = (c_{A\uparrow}^\dagger(k), c_{B\uparrow}^\dagger(k), c_{A\downarrow}^\dagger(k), c_{B\downarrow}^\dagger(k), c_{A\downarrow}(-k), c_{B\downarrow}(-k), c_{A\uparrow}(-k), c_{B\uparrow}(-k)), \tag{3}$$

so the time reversal operator is given by $\mathcal{T} = is_y\tau_0\sigma_0 K$, where K is the complex conjugation operator, and s_j, τ_j, and σ_j are Pauli matrices acting on spin, particle-hole, and pseudospin sublattices, respectively, with $j = 0, x, y, z$. Notice that the BdG system is particle-hole symmetric, as it satisfies $\mathcal{C}\mathcal{H}_{\rm BdG}(k)\mathcal{C}^{-1} = -\mathcal{H}_{\rm BdG}(-k)$, where $\mathcal{C}$ is the particle-hole exchange operator [13]. Let us now introduce the minimal model Hamiltonian of TMD-proximitized graphene represented by $\mathcal{H}_e$.

A. Topological phases of proximitized graphene

The Hamiltonian of proximitized graphene includes perturbations that describe the use of TMD as substrate material [26–29,33]. As such, the graphene system includes staggered (Δ), intrinsic SOC (S), pseudo-Zeeman SOC (L), and Rashba SOC (R) terms that can be described as follows:

$$\mathcal{H}_e(k) = \begin{pmatrix} \Delta + (S+L)f(k) & T(k) & 0 & R(k) \\ T(k)^\dagger & -\Delta - (S-L)f(k) & R(-k) & 0 \\ 0 & R(-k)^\dagger & \Delta - (S+L)f(k) & T(k) \\ R(k)^\dagger & 0 & T(k)^\dagger & -\Delta + (S-L)f(k) \end{pmatrix}, \tag{4}$$

written in the basis $\phi_k = (A\uparrow, B\uparrow, A\downarrow, B\downarrow)^T$, where k is the 2D momentum space vector measured from the Γ point and

$$T(k) = t(1 + e^{ik\cdot a_1} + e^{ik\cdot a_2}), \quad R(k) = \frac{-i}{3}R(1 + e^{-i\phi}e^{ik\cdot a_1} + e^{i\phi}e^{ik\cdot a_2}), \quad f(k) = \frac{-2}{3\sqrt{3}}[\sin(k\cdot a_1) - \sin(k\cdot a_2) + \sin(k\cdot a_3)], \tag{5}$$

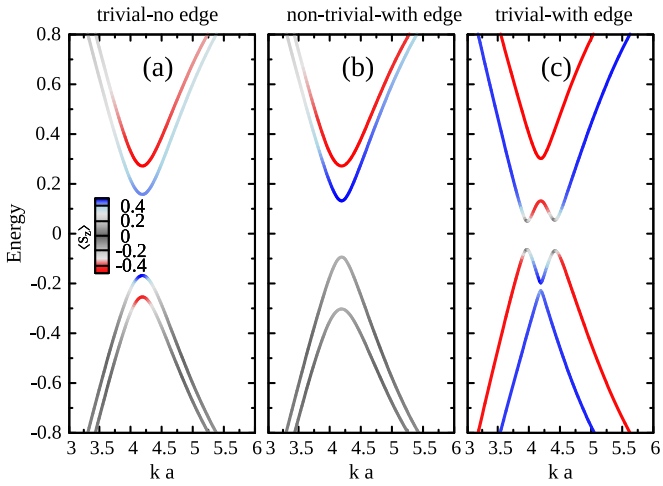

FIG. 1. Band structure near the Brillouin zone K point of TMD-proximitized graphene Hamiltonian in Eq. (4). Panels show (a) direct and (b) topological band-gap system where the larger staggered Δ (a) or intrinsic SOC S (b) interaction term is largest and causes the system gap. Consequently, the left (middle) panel describes a trivial (nontrivial) topological phase, in which edge states are absent (present) in finite systems. Panel (c) shows system with inverted bands, dominated by the pseudo-Zeeman interaction L. This phase exhibits edge states, even when it is topologically trivial. Red (blue) describes the spin-up (-down) S_z spin projection for these bands—-see scale in (a). Parameters (Δ, S, L) used for each phase are (a) direct gap (0.2, 0.05, 0.02), (b) QSH phase (0.05, 0.2, 0.02), (c) inverted mass phase (0.05, 0.05, 0.2). All panels include the same Rashba SOC, $R = 0.1$. Energies in units of NN hopping constant t.

with $\phi = \frac{2\pi}{3}$, and a_j are the real space vectors which define the unit cell of graphene,

$$a_1 = a(1, 0),$$
$$a_{2,3} = a(1/2, \pm\sqrt{3}/2), \tag{6}$$

where $a = 2.46$ Å is the lattice constant. The two Dirac cones at K and K' symmetry points of the Brillouin zone are at $(\pm\frac{4\pi}{3a}, 0)$. In the rest of this paper, we will set the NN hopping constant $t \simeq 3$eV as the unit of energy.

The competition between different perturbations leads to three distinct topological electronic phases in the Hamiltonian of Eq. (4), which we now briefly discuss [29–31]. First, a direct band-gap regime, in which the system is topologically trivial, is obtained when the Hamiltonian is dominated by the staggered potential Δ [34]. A second gapped regime that is topologically nontrivial and exhibits QSH effect with two propagating edge states is obtained when the intrinsic SOC S term dominates [31]. The third gapped regime of inverted mass bands is obtained when the pseudo-Zeeman perturbation L dominates; this regime also exhibits conducting edge states, although of a different type, while having a trivial topological structure [28,30]. Examples of these three phases are shown in Fig. 1. They can be reached in experiments by exploring different TMDs, relative twist, or voltage potential between the layers, as well as external pressure, as the various Hamiltonian parameters change differently with external environmental fields [28]. Transitions between these phases require closing of the gap as parameters change.

B. Superconductivity order parameter

Several studies have been carried out to study possible superconducting order parameters in the graphene honeycomb lattice, their symmetries, and topological properties [13,15], with some controversial results [6]. Differences in doping level and symmetries of interactions in such systems result in a variety of interesting QP spectra. For instance, studies have found a significant contribution to the superconducting correlations involving NNs and NNNs in the lattice as s-wave, f-wave, or even d-wave symmetries are present [6,35]. In this paper, we study systems with singlet and triplet pairing functions for coupling involving both NNs and NNNs. The pairing matrix $\hat{\Gamma}$ in Eq. (1) for different symmetries can be described in terms of effective coupling amplitude functions given by [6,35]

$$\begin{aligned}
\gamma_s^{\mathrm{NN}}(k) &= \gamma \sum_{n=1}^{3} e^{ik\cdot\delta_n}, \\
\gamma_f^{\mathrm{NN}}(k) &= \gamma \sum_{n=1}^{3} \nu_n e^{ik\cdot\delta_n}, \\
\gamma_s^{\mathrm{NNN}}(k) &= \gamma \sum_{n=1}^{6} e^{ik\cdot a_n}, \\
\gamma_f^{\mathrm{NNN}}(k) &= \gamma \sum_{n=1}^{6} (-1)^n e^{ik\cdot a_n},
\end{aligned} \tag{7}$$

with γ characterizing the strength of the superconducting pairing. The first two lines describe s- and f-wave symmetry coupling between NNs (A and B sublattices). The third and fourth lines describe the corresponding s- and f-wave potentials for NNN sites. Here, the lattice vector a_n connects A/B to its NNN, the same sublattice in the neighboring unit cell; $\nu_n = +1(-1)$ if the hopping is from A to B (B to A); δ_n describes the three vectors that connect A-B NN sites in the lattice.

The choices of pairing symmetries are consistent with the trigonal symmetry of the honeycomb lattice structure. Singlet pairings, such as $\hat{\Gamma} = i\sigma_x s_y \gamma_s^{\mathrm{NN}}$, have even parity under spatial inversion, whereas the triplet pairings, e.g., $\hat{\Gamma} = -i\sigma_y s_x \gamma_f^{\mathrm{NN}}$, are odd. Hence, these two pairings do not "mix" in lattices with inversion symmetry. As the effective Hamiltonian considered here breaks such symmetry, it allows the overlap between these two pairing order parameters [8]. For simplicity and ease of analysis, we consider the two symmetries separately, and discuss later on the case of mixed symmetry.

III. RESULTS AND DISCUSSION

As described above, the proximitized graphene system exhibits three distinct gapped topological phases that cannot be smoothly deformed into each other without closing the single-particle excitation gap [28]. Correspondingly, the BdG Hamiltonian inherits the single-particle spectral properties. The resulting QP excitation spectrum exhibits phases with

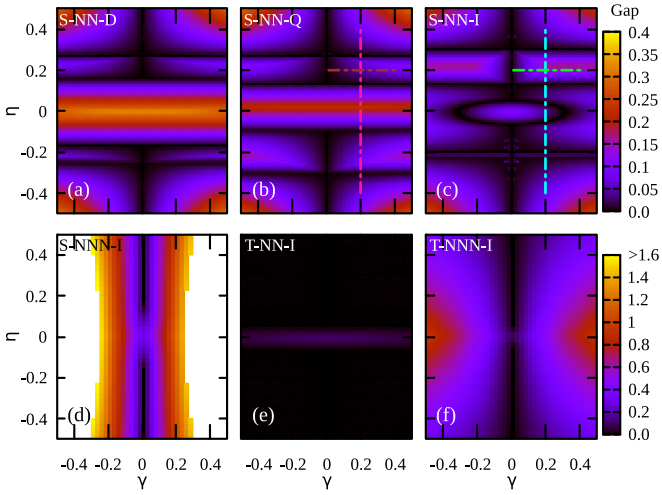

FIG. 2. Map of QP gap for different proximitized graphene superconducting phases as function of chemical potential η and pairing strength γ. The scale of the gap for each panel row is shown on right. Top three panels show phases for nearest-neighbor s-wave pairing for (a) direct (S-NN-D), (b) QSH (S-NN-Q), and (c) inverted (S-NN-I) phases. The bottom middle panel (e) shows the near absence of gap for the inverted band phase with NN f-wave pairing (T-NN-I). Also shown are gaps for the inverted mass Hamiltonian for NNN (d) s-wave (S-NNN-I), and (f) f-wave (T-NNN-I). Vertical and horizontal dashed-dot lines in panels indicate cross sections shown in Figs. 3–5. Energies in units of NN hopping constant t.

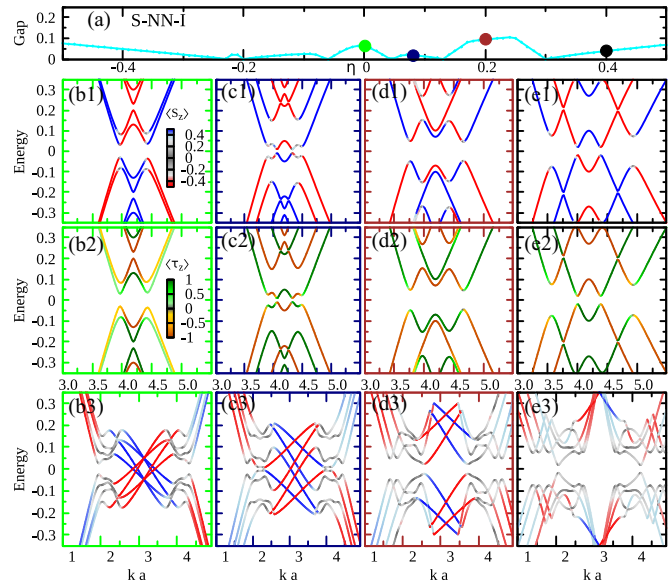

FIG. 3. (a) QP spectral gap of the BdG Hamiltonian of graphene modulated by NN s-wave pairing for inverted mass regime at fixed strength $\gamma = 0.2$ vs chemical potential η, as indicated by the vertical cyan line in Fig. 2(c). Different QP spectra at few selected η values are shown in the panels below with frame color coded; (b1)–(e1) show S_z spin projections of the QP spectra; (b2)–(e2) show corresponding τ_z particle-hole projection. Notice complex QP spin and particle-hole structure evolves as η changes, suggesting different Berry curvatures across gap closing events. (b3)–(e3) show low-energy spectra for zigzag ribbons in each corresponding parameter regime. Robust metallic edge states are seen in (b3) and (c3), which become hybridized with bulk states in (d3) and (e3). Energies in units of NN hopping constant t.

interesting Berry curvature features that cannot be smoothly deformed into different phases without first closing the QP gap. We exploit here this necessary (but insufficient) condition for a phase transition and explore the possible phases that the BdG Hamiltonian could exhibit upon variation of chemical potential and/or strength of the superconducting pairing. We study as well how the s or f symmetry of the $\hat{\Gamma}$ matrix affects the QP spectrum.

After exploring the excitation gap as a function of parameters for different regimes, we identify the topological character of such phases.

A. Quasiparticle spectra and pairing symmetries

As the BdG Hamiltonian preserves particle-hole symmetry, the QP bands must be symmetric around zero energy, which allows for band crossings. As expected, the QP gap typically lies close to (but not at) high symmetry points in reciprocal space, moving around as γ and η values vary. Figure 2 shows the η-γ dependence of the minimal spectral gap for the system in the direct, QSH, and inverted phases for different singlet and triplet superconducting pairing functions. We have analyzed different coupling parameters and phases, and focus the discussion here on few regimes that show interesting features; other parameter sets behave in a similar fashion.

The behavior of the gap function for NN pairing exhibits qualitative differences between the singlet and triplet symmetries. The QP gap dependence for NN singlet s-wave pairing potential is different in the different single-particle regimes. The gap is symmetric around $\gamma = 0$, as well as being particle-hole symmetric, as expected. For γ and η near zero, the QP gap is not zero, reflecting the single-particle gap in the spectrum seen in Fig. 1, and inherited by the superconducting phase, as seen in the top panels of Fig. 2. Notice that as the absolute value of the chemical potential increases, the gap has interesting behavior, closing at specific values and having nonmonotonic dependence on the γ parameter. Notice the QP gap is not symmetric under η reversal, which reflects the structure asymmetry of the single-particle spectra seen in Fig. 1.

To better understand the behavior of the system under changing chemical potential, Fig. 3 shows the gap of the superconducting system versus η along vertical lines (red and cyan) in Figs. 2(b) and 2(c), as well as the corresponding QP spectrum near the K symmetry point for selected parameter sets. Notice that the spectral structures are separated by gap closing points as η changes, suggesting one to look for possible changes in topology across those values.

Figure 3(a) shows the gap size as a function of η for the inverted mass system of Fig. 2(c) [and single-particle spectrum in Fig. 1(c)]. The QP gap for $\eta \simeq 0$ (green dot) is nearly the same size as the single-particle spectral gap—-even as $\gamma = 0.2$ here. As η increases, however, the QP bands begin to overlap (blue dot) and a smaller superconducting gap appears. The QP spectrum has increasingly distorted curvatures, as seen in Figs. 3(c1) and 3(c2), as the inverted bands are increasingly mixed by the pairing function, as shown in subsequent

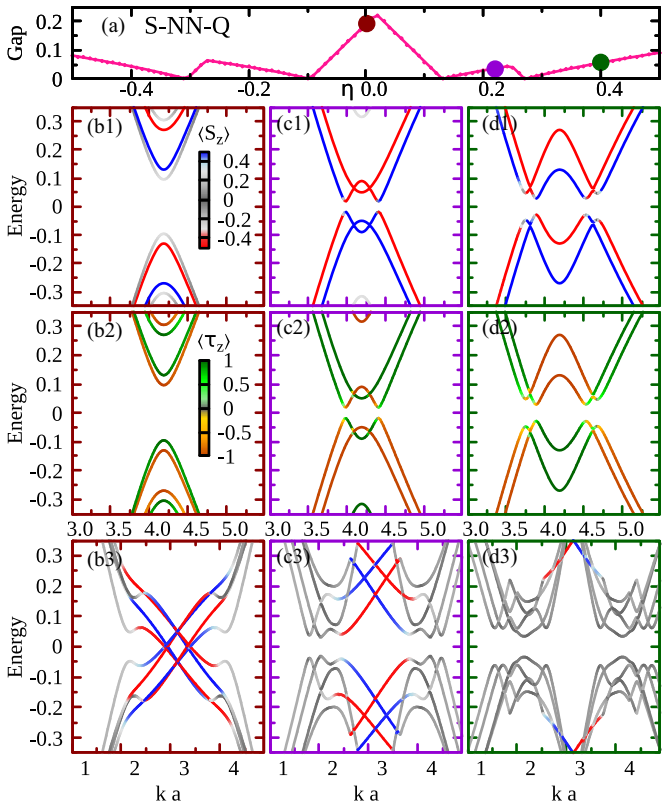

FIG. 4. (a) QP spectral gap of the BdG Hamiltonian of graphene modulated by NN s-wave pairing for QSH regime at fixed strength $\gamma = 0.2$ versus chemical potential η, as indicated by red vertical line in Fig. 2(b). Different QP spectra at selected η values are shown in the panels below and color coded. (b1)–(d1) show S_z spin projections of the QP spectra; (b2)–(d2) show corresponding τ_z particle-hole projections. (b3)–(d3) show low-energy spectra for zigzag ribbons in each corresponding parameter regime. Metallic edge state are clear in (b3). Energies in units of NN hopping constant t.

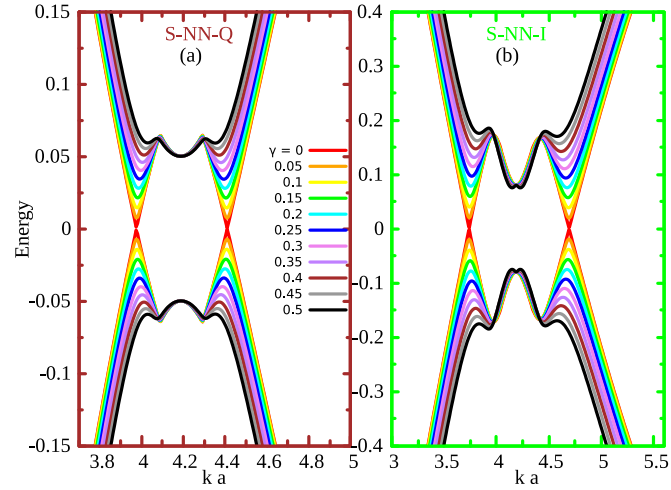

FIG. 5. QP spectral edge near the gap for BdG superconductor with NN s-wave pairing in proximitized graphene at constant $\eta = 0.2$, as shown by horizontal lines in Figs. 2(b) and 2(c), for different γ values indicated in left panel. (a) describes system in QSH phase; (b) system in inverted mass phase. Notice states at the K symmetry point are only slightly affected by γ. Energies in units of NN hopping constant t.

panels of Fig. 3. Notice the spectral gap is largest for $\eta \simeq 0.2$, seemingly associated with the maximum of the inverted conduction band segment in Fig. 1(c). Figures 3(b1) and 3(b2) show the spin and particle-hole components, respectively, for $\eta = 0$, showing how the superconducting pairing produces mixed τ_z values. Differences appear in both the spin and particle-hole structure as η changes. The spin textures of the single-particle spectrum are essentially preserved, except in the band overlap/crossing region, where the pairing function causes evident mixing. As the QP gap changes with η, we see in Figs. 3(d) and 3(e) that particle-hole mixing is mostly present near the QP gap, as one could expect. Yet, in Fig. 3(d2) we notice clear particle-hole mixing even at $E \simeq \pm 0.3$ (here $\gamma = 0.2 \simeq \eta$) illustrating the importance of the single-particle spin textures strongly affecting the superconducting correlations. In contrast, Figs. 3(c2) and 3(e2) show no particle-hole mixing beyond the QP gap region. The system preserves time-reversal symmetry, with the corresponding inverted spectrum around the K' point (not shown).

Figure 4(a) considers a different system, where the superconducting gap versus η in the QSH phase of Fig. 1(b) is shown, along the red vertical line in Fig. 2(b) at $\gamma = 0.2$. For $\eta \simeq 0$, the spectral gap is essentially that given by the single-particle gap ($\gtrsim \gamma$), showing nearly no particle-hole mixing, as seen in Fig. 4(b2). As η increases to $\simeq 0.2$ (purple dot), we notice that the spin structure in Fig. 1(b) and the symmetry-breaking Rashba field give rise to a region of inverted mass QPs with interesting spin texture and clear particle-hole mixing near the gap edges. After a gap-closing event at $\eta \simeq 0.27$, the gap increases again (green dot) with near gap spin projections reversed from before, and concomitantly inverted Berry curvature [Fig. 4(d1)]. Similarly, the particle-hole projections appear strongly mixed near the QP gap edges in Fig. 4(d2).

We now analyze how the superconducting pairing strength changes the system. Figure 5 shows the QP spectral edge near the energy gap for different γ values and constant η [$= 0.2$, horizontal lines in Figs. 2(b) and 2(c)]. The gapless spectra at $\gamma = 0$ develop a superconducting gap as γ increases, at points near each K and K' valley. The gap grows as the pairing strength increases at those k momenta, whereas the states at K change only slightly with γ. One observes in the QSH phase (left panel), that the parabolic band edges at the K point remain essentially unchanged for all γ parameters, whereas in the inverted band case (right panel), the once parabolic bands convert into slightly inverted bands around the symmetry point. Notice that the increasing gap with larger γ eventually saturates, as seen in Fig. 2, as the the smallest overall gap shown there is more a reflection of the single-particle spectrum at large γ.

Figure 2(e) shows that the gap for the triplet NN f-wave superconductor vanishes nearly for all values of chemical potential, with the system having a gap only for values of η around zero (essentially the particle gap), while γ does not induce much change. This puzzling gapless superconducting state is reminiscent of the "hidden order" reported for p-wave symmetry in graphene [36], which here surprisingly persists for all the single-particle regimes of the proximitized

graphene Hamiltonian. Figure 2 also shows representative examples of the (d) NNN singlet and (f) triplet pairing, both in the inverted mass regime of Fig. 1(c). These phases exhibit similar qualitative behavior for all three topological Hamiltonian regimes. For NNN coupling, for example, the QP gap increases monotonically as γ increases, as seen in Figs. 2(d) and 2(f) [37].

Finally, we should also comment that as the proximitized graphene lacks spatial inversion, the superconducting state could include a mixture of *s*- and *f*-wave symmetries, as mentioned above. We have analyzed cases where both γ_s and γ_f are present. The resulting QP spectra acquires the main features of the dominant pairing, smoothly evolving between the two symmetries (not shown).

B. Topological invariants and edge states of SC gapped phases

We now analyze the topological invariants of the gapped superconducting system in the different phases. The Hamiltonian in Eq. (1), as described, preserves time-reversal and particle-hole symmetries. Hence, the 2D proximitized graphene system belongs to the DII topological class and its Z_2 topological invariant determines the character of the states [13,38]. Most important is that the nontrivial system cannot be adiabatically connected to vacuum states and, to do so, the excitation band gap needs to close. The Z_2 index for the different superconducting topological phases in this system has been calculated using the Z2PACK [39]. This convenient method allows calculating the topological invariant starting from the BdG tight-binding model in Eq. (1).

We find that Z2PACK identifies *all* of the superconducting gapped phases to be topologically trivial states. This classification is true for all three single particle regimes (direct, inverted mass, and QSH) and all pairing symmetries considered here. One would have expected that the nontrivial nature of the single-particle states in at least the QSH be carried forward in the superconducting regime. However, the trivial topology obtained in the BdG Hamiltonian is understood as arriving from the presence of the two Dirac-like bands separated in momentum space and related to each other by time-reversal symmetry.

Study of the edge states in a finite system provides another way to analyze the trivial topology of these systems. We use a zigzag nanoribbon of the proximitized graphene system in the appropriate regime [32,33,40] to obtain the QP spectrum. The appearance of gapless edge states is a characteristic feature of nontrivial topological phases, as per the bulk-boundary correspondence. According to the anticipated trivial character, we find no propagating edge states for systems with NNN singlet and triplet SC pairing. Edge states are fully gapped as well for NN singlets when in the direct gap regime.

However, interestingly different results are found in systems with NN singlet pairing for either the QSH or inverted regimes, showing interesting metallic edge states closely related with those in the particle Hamiltonian in each phase. These features can be seen in the QP spectrum for the zigzag nanoribbon of each system/regime in the bottom panels of Figs. 3 and 4. Each panel in the bottom row corresponds to the different η values as indicated by the color dots above. In Figs. 3(b3) and 3(c3), corresponding to $\eta \simeq 0$, and 0.2, one finds eight spin-polarized edge states propagating across the gap. These eight mixed electron and hole states exist localized at the zigzag boundaries of the system. As η increases, Figs. 3(d3) and 3(e3), the localized edge modes evolve to be hybridized with the bulk, and eventually spread over the whole nanoribbon structure. Notice that after the gap closing event for $\eta \gtrsim 0.15$ in systems with inverted mass, the metallic edge states disappear.

In Fig. 4, the corresponding bottom row shows no metallic edge states, except for $\eta \simeq 0$, in Fig. 4(b3). Again, as η increases, the edge states promptly hybridize with the bulk QPs.

It is interesting to more closely analyze the origin of these edge states by looking at the eigenvector components. In Fig. 3(c3), we find that the constituents of these edge modes are from only one sublattice, i.e., A_{e1} and A_{h1}, where the spin is implicit and e (h) stands for electron (hole) components of the BdG spinor. This behavior is reminiscent of that for zigzag edges in graphene. Two of these four bands must be associated with the hole part of the electron components due to the preserved time-reversal symmetry.

We emphasize that regardless of the presence of metallic edge states in different η and γ parameter ranges, there is no true topological phase transition, since the superconducting states are all characterized by a trivial topological invariant. However, the presence of these well-defined edge states are the consequence of the structural protection afforded by the honeycomb lattice.

C. Possible experimental systems

Several experimental designs to induce superconductivity onto monolayer or few-layer systems have been reported successfully over the last decade [2,41]. For example, monolayer MoS_2 has been shown to be superconductor upon strong gating [42,43]. Moreover, studies have shown *s*-wave proximity-induced superconductivity in a MoS_2 monolayer when on a Pb thin film substrate, with a sizable gap measured by STM [44]. A TMD monolayer with Zeeman-like SOC is shown theoretically to allow spin-triplet pairings and induce superconductivity in a half-metallic wire by proximity [45]. These results suggest that using intrinsic superconductor materials with strong Zeeman-like SOC such as $NbSe_2$ would provide a suitable platform to explore the model systems we study here. Recent success on sandwiching graphene by different other monolayers (including BN and different TMDs, as discussed in the Introduction) have also enhanced the experimental possibilities.

We note that the symmetries and nature of the emerging superconducting gap are distinct in different structures, as the various single-particle spectra contribute differently once the pairing is present. Hence, the possibility of tuning the parameters in a given material system via the application of gate voltages or relative layer twists to induce superconducting gaps with different intriguing symmetries is very attractive. We trust this versatility will motivate further exploration in different labs.

IV. CONCLUSION

We have studied theoretically the role of superconducting pairing interactions in proximitized graphene that may be in

one of three distinct topological phases. These all feature massive Dirac fermions with tunable band gap and different band curvatures, due to the competition of different spin-orbit and staggered potential terms in the Hamiltonian. We have considered pairing functions with singlet *s*-wave and triplet *f*-wave symmetries on the generalized honeycomb lattice graphene model, considering NN and NNN couplings.

Despite the topologically different single-particle band structure of proximitized graphene, we have found that all superconducting regimes studied here are topologically trivial, as determined by their Z_2 index. This result arises from the presence of time-reversed pairs of Dirac points in graphene and the corresponding symmetry in the BdG Hamiltonian, and remains valid over the entire range of chemical potential η and pairing strength γ we studied.

In the QSH and inverted bands phases of the system, the superconducting *s*-wave correlations produce interesting behavior. Both phases, although topologically trivial, are shown to exhibit robust edge states, which eventually gap and hybridize with bulk states after gap-closing transition, as the chemical potential in the system is shifted. It would be interesting to see this behavior in experimental systems where the Fermi level can be controlled over a suitable range.

ACKNOWLEDGMENT

We thank discussions with M. M. Asmar.

[1] A. H. Castro Neto, F. Guinea, N. M. R. Peres, K. S. Novoselov, and A. K. Geim, Rev. Mod. Phys. **81**, 109 (2009).
[2] H. B. Heersche, P. Jarillo-Herrero, J. B. Oostinga, L. M. Vandersypen, and A. F. Morpurgo, Solid State Commun. **143**, 72 (2007).
[3] J. P. L. Faye, P. Sahebsara, and D. Sénéchal, Phys. Rev. B **92**, 085121 (2015).
[4] K. Halterman, O. T. Valls, and M. Alidoust, Phys. Rev. Lett. **111**, 046602 (2013).
[5] M. Alidoust, M. Willatzen, and A.-P. Jauho, Phys. Rev. B **99**, 155413 (2019).
[6] T. Ying and S. Wessel, Phys. Rev. B **97**, 075127 (2018).
[7] T. Watanabe and S. Ishihara, J. Phys. Soc. Jpn. **82**, 034704 (2013).
[8] M. M. Asmar and S. E. Ulloa, Phys. Rev. B **91**, 165407 (2015).
[9] A. K. Geim and I. V. Grigorieva, Nature **499**, 419 (2013).
[10] S. Ebadzadeh, H. Goudarzi, and M. Khezerlou, Phys. B: Condens. Matter **559**, 32 (2019).
[11] Y. S. Gani, H. Steinberg, and E. Rossi, Phys. Rev. B **99**, 235404 (2019).
[12] S. Ray, J. Jung, and T. Das, Phys. Rev. B **99**, 134515 (2019).
[13] M. Sato and Y. Ando, Rep. Prog. Phys. **80**, 076501 (2017).
[14] Y.-T. Hsu, A. Vaezi, M. H. Fischer, and E.-A. Kim, Nat. Commun. **8**, 14985 (2017).
[15] K. Lee, T. Hazra, M. Randeria, and N. Trivedi, Phys. Rev. B **99**, 184514 (2019).
[16] F. Zhang, C. L. Kane, and E. J. Mele, Phys. Rev. Lett. **111**, 056402 (2013).
[17] J. Linder and T. Yokoyama, Phys. Rev. B **89**, 020504(R) (2014).
[18] Y. Cao, V. Fatemi, A. Demir, S. Fang, S. L. Tomarken, J. Y. Luo, J. D. Sanchez-Yamagishi, K. Watanabe, T. Taniguchi, E. Kaxiras, R. C. Ashoori, and P. Jarillo-Herrero, Nature **556**, 80 (2018).
[19] M. Yankowitz, S. Chen, H. Polshyn, Y. Zhang, K. Watanabe, T. Taniguchi, D. Graf, A. F. Young, and C. R. Dean, Science **363**, 1059 (2019).
[20] H. S. Arora, R. Polski, Y. Zhang, A. Thomson, Y. Choi, H. Kim, Z. Lin, I. Z. Wilson, X. Xu, J.-H. Chu, K. Watanabe, T. Taniguchi, J. Alicea, and S. Nadj-Perge, Nature **583**, 379 (2020).
[21] Z. Wang, D.-K. Ki, J. Y. Khoo, D. Mauro, H. Berger, L. S. Levitov, and A. F. Morpurgo, Phys. Rev. X **6**, 041020 (2016).
[22] Z. Wang, D.-K. Ki, H. Chen, H. Berger, A. H. MacDonald, and A. F. Morpurgo, Nat. Commun. **6**, 8339 (2015).
[23] J. O. Island, X. Cui, C. Lewandowski, J. Y. Khoo, E. M. Spanton, H. Zhou, D. Rhodes, J. C. Hone, T. Taniguchi, K. Watanabe, L. S. Levitov, M. P. Zaletel, and A. F. Young, Nature **571**, 85 (2019).
[24] G.-B. Liu, W.-Y. Shan, Y. Yao, W. Yao, and D. Xiao, Phys. Rev. B **88**, 085433 (2013).
[25] J. R. Schaibley, H. Yu, G. Clark, P. Rivera, J. S. Ross, K. L. Seyler, W. Yao, and X. Xu, Nat. Rev. Mater. **1**, 16055 (2016).
[26] M. Gmitra and J. Fabian, Phys. Rev. B **92**, 155403 (2015).
[27] M. Gmitra, D. Kochan, P. Högl, and J. Fabian, Phys. Rev. B **93**, 155104 (2016).
[28] A. M. Alsharari, M. M. Asmar, and S. E. Ulloa, Phys. Rev. B **98**, 195129 (2018).
[29] A. M. Alsharari, M. M. Asmar, and S. E. Ulloa, Phys. Rev. B **94**, 241106(R) (2016).
[30] T. Frank, P. Högl, M. Gmitra, D. Kochan, and J. Fabian, Phys. Rev. Lett. **120**, 156402 (2018).
[31] C. L. Kane and E. J. Mele, Phys. Rev. Lett. **95**, 226801 (2005).
[32] L. Wang and M. W. Wu, Phys. Rev. B **93**, 054502 (2016).
[33] A. M. Alsharari, M. M. Asmar, and S. E. Ulloa, Phys. Rev. B **97**, 241104(R) (2018).
[34] D. Xiao, W. Yao, and Q. Niu, Phys. Rev. Lett. **99**, 236809 (2007).
[35] L.-Y. Xiao, S.-L. Yu, W. Wang, Z.-J. Yao, and J.-X. Li, Europhys. Lett. **115**, 27008 (2016).
[36] B. Uchoa and A. H. Castro Neto, Phys. Rev. Lett. **98**, 146801 (2007).
[37] Chiral superconductivity and associated edge states require broken time-reversal symmetry, whereas the *f* wave we consider preserves that symmetry [46].
[38] A. Altland and M. R. Zirnbauer, Phys. Rev. B **55**, 1142 (1997).
[39] D. Gresch, G. Autès, O. V. Yazyev, M. Troyer, D. Vanderbilt, B. A. Bernevig, and A. A. Soluyanov, Phys. Rev. B **95**, 075146 (2017).
[40] C. Dutreix, M. Guigou, D. Chevallier, and C. Bena, Eur. Phys. J. B **87**, 296 (2014).

[41] H. B. Heersche, P. Jarillo-Herrero, J. B. Oostinga, L. M. Vandersypen, and A. F. Morpurgo, Nature **446**, 56 (2007).

[42] E. Piatti, D. De Fazio, D. Daghero, S. R. Tamalampudi, D. Yoon, A. C. Ferrari, and R. S. Gonnelli, Nano Lett. **18**, 4821 (2018).

[43] D. Costanzo, H. Zhang, B. A. Reddy, H. Berger, and A. F. Morpurgo, Nat. Nanotech. **13**, 483 (2018).

[44] D. J. Trainer, B. Wang, F. Bobba, N. Samuelson, X. Xi, J. Zasadzinski, J. Nieminen, A. Bansil, and M. Iavarone, ACS Nano **14**, 2718 (2020).

[45] B. T. Zhou, N. F. Q. Yuan, H.-L. Jiang, and K. T. Law, Phys. Rev. B **93**, 180501(R) (2016).

[46] J.-L. Zhang, W. Huang, M. Sigrist, and D.-X. Yao, Phys. Rev. B **96**, 224504 (2017).